View Article Online
View Journal

Green Chemistry

Cutting-edge research for a greener sustainable future

Accepted Manuscript

This article can be cited before page numbers have been issued, to do this please use: X. Chen, H. Zhao, J. Qu, D. Tang, Z. Zhao, H. Xie, D. Wang and H. Yin, *Green Chem.*, 2020, DOI: 10.1039/D0GC02626C.

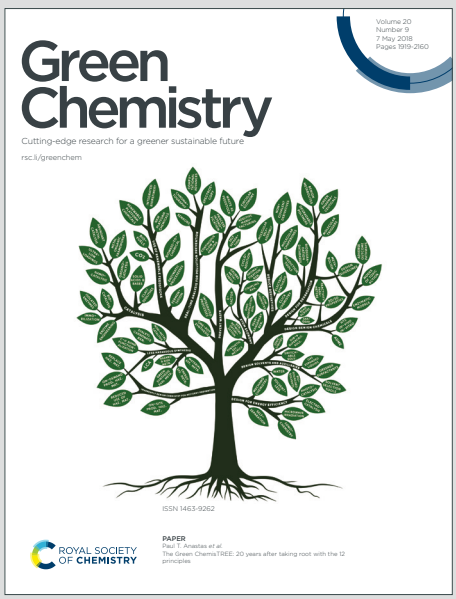

View Article Online
DOI: 10.1039/D0GC02626C

A molten calcium carbonate mediator for the electrochemical conversion and absorption of carbon dioxide

Xiang Chen[1], Haijia Zhao[1], Jiakang Qu[1], Diyong Tang[2], Zhuqing Zhao[1], Hongwei Xie[1], Dihua Wang[2], Huayi Yin*[1,3]

1. Key Laboratory for Ecological Metallurgy of Multimetallic Mineral of Ministry of Education, School of Metallurgy, Northeastern University, Shenyang, P. R. China, 110819

2. School of Resource and Environmental Science, Wuhan University, Wuhan, P.R. China, 430072

3. Key Laboratory of Data Analytics and Optimization for Smart Industry, Ministry of Education, Northeastern University, Shenyang, P. R. China,110819

Email: yinhy@smm.neu.edu.cn

Abstract: High-temperature molten salts are an excellent electrolyte to entail redox reactions at a rapid rate without using rationally designed nano-structured catalysts. However, the large-scale electrolyzer is constrained by expensive and resource-deficient lithium salts. Employing earth-abundant $CaCO_3$ releases the pressure of using strategic lithium resources, but the low solubility of CaO in molten carbonates disables the capability of capturing CO_2. In addition, the separation of carbon from water-insoluble CaO and $CaCO_3$ consumes a large amount of acids. To tackle these challenges, we report a $CaCO_3$-containing molten carbonate electrolyzer to prevent the use of lithium salt, and a molten $CaCl_2$ dissolver to separate carbon from CaO that is soluble in molten $CaCl_2$ and can capture CO_2 by carbonization. More importantly, we develop a salt-soluble-to-water-insoluble approach to producing ultrafine $CaCO_3$ by using molten salt as a soft template. Overall, this paper opens a pathway to use the cheap and earth-abundant molten $CaCO_3$ as a mediator to converting CO_2 to oxygen at a cost-effective inert

View Article Online
DOI: 10.1039/D0GC02626C

anode, value-added carbon at the cathode, and ultrafine $CaCO_3$ thorough a salt-to-solution process.

Keywords: $CaCO_3$, molten carbonate, electrolysis, CO_2 reduction, carbon materials

1. Introduction

Electrochemical valorization of CO_2 is the key to closing the carbon cycle and achieving global sustainability. Using renewable energy-powered electrolyzers to capture and reduce carbon dioxide is becoming a central focus to balancing the carbon cycle and therefore tacking the climate change[1]. With the ever-decreasing cost of renewable energies, almost reaching the cost-level of fossil-generated power[2, 3], electrochemically converting CO_2 to value-added chemicals and fuels gradually becomes commercially viable[4-6]. Most state-of-the-art electrochemical technologies aim to convert gaseous CO_2 to CO or organic chemicals in aqueous solutions where water molecules provide the protons and electrons give energy to form new chemical bonds[4]. However, the electrochemical conversion of CO_2 in aqueous solutions needs to rationally design catalysts, engineer the electrolyte/electrode interface, and employ gas diffusion electrode to improve the product selectivity and increase the relatively low current density caused by the low solubility of CO_2 in aqueous solutions[7, 8]. In addition to atmospheric CO_2 (~2.5×10^{12} tones), a larger portion of CO_2 exists in the carbonate rocks (~10^{14} tones) and the hydrosphere (~10^{16} tones)[9, 10]. Thus, solid carbonate minerals are another primary CO_2 carrier. The electrochemical conversion of carbonate minerals could be another avenue to valorize CO_2 by using feedstocks that are available and being easily concentrated, and the dissociation of carbonate will generate basic oxide being capable of capturing CO_2 through

View Article Online
DOI: 10.1039/D0GC02626C

carbonization or being directly used as raw materials for cement production[11].

In addition to aqueous solutions, high-temperature molten salts have been proven as excellent electrolytes to convert CO_2 to carbons or hydrocarbons if water vapor was supplied[12-18]. Unlike the aqueous solution, high-temperature molten salts have a wider electrochemical window than that of water to allow the conversion CO_2 to carbon with a high product selectivity, and the high operating temperature overcomes the kinetic barrier and thereby enables a rapid reduction rate without tentatively designed catalysts. For example, the industrially deployed Hall-Heroult process for producing liquid aluminum has been commercialized for ~100 years. However, the solubility of CO_2 in molten salts is still low[19, 20], so the direct electrochemical reduction of gaseous CO_2 cannot be sustained at a high current density. Different from aqueous solutions, the carbonate anions can be reduced to carbon in molten salt while releasing oxide into the molten salt to capture CO_2 and then replenish CO_3^{2-} ions. In this case, the rates of generating oxide, the dissolution of oxide in molten salt, and the carbonation of oxide should be balanced to avoid any polarization or side reactions in addition to producing carbon. To date, most researches focus on lithium-containing molten carbonates due to their relatively low melting point and acceptable oxide solubility (**Tab. S1**)[12-18]. However, the lithium resource is limited because of the ever-increasing lithium-ion battery market[21, 22]. Thus, a lithium-free and earth-abundant molten carbonate salt is required in terms of considering the large-scale deployment and the cost requirement of raw materials.

Calcium carbonate, the primary constituent of limestone, is cheap, earth-abundant, environmentally friendly, and easily accessible, which covers ~15% of the continental surface[23, 24]. This means that the limestone is a huge CO_2 reservoir[25]. On the other hand, the limestone

View Article Online
DOI: 10.1039/D0GC02626C

could act as an abundant medium performing the CO_2 transformation. Licht et al. have proved that $CaCO_3$ can be reduced to C and CaO in Li_2CO_3-containing molten salt[26]. However, the solubility of CaO is very low in ternary molten carbonate (Na_2CO_3-K_2CO_3-Li_2CO_3 eutectic), and the solubilities of both $Ca(OH)_2$ (0.173 g/100g-H_2O, 20 ^oC) and $CaCO_3$ (0.0006 g/100g-H_2O, 20 ^oC) in water are small, so that the separation of the electrolytic products from molten salt consumes a large amount of water and acids. Thus, a lithium-free molten carbonate electrolyzer and an efficient separation method to separate CaO or $CaCO_3$ from the electrolytic carbon are urgently needed.

To circumvent the challenge of using lithium salts and the difficulty of product separation, herein we employ a lithium-free molten carbonate, $CaCO_3$-Na_2CO_3-K_2CO_3, to convert molten $CaCO_3$ to solid carbon and CaO at the cathode and oxygen at a low-cost Ni10Cu11Fe inert anode. Subsequently, the CaO and carbon can be separated in molten $CaCl_2$ because both CaO and $CaCO_3$ are highly soluble in molten $CaCl_2$[27, 28]. Since both CaO and $CaCO_3$ are highly soluble in molten $CaCl_2$, the CaO can be either separated by water leaching or directly used for absorbing CO_2 by carbonization. Moreover, the ultrafine $CaCO_3$ with a diameter ranging from 500 to 800 nm can be obtained by a soft template approach, in which $CaCO_3$ is highly soluble in molten $CaCl_2$ while $CaCO_3$ is insoluble in water but $CaCl_2$ is highly soluble in water. Because $CaCO_3$ can be substituted by the limestone, we use the cheap limestone as a CO_2 host to enable the electrochemical conversion of CO_2 to value-added carbon materials and oxygen. Finally, the sodium-storage performances of the electrolytic carbon were evaluated as well.

2. Experimental

2.1 Electrochemistry of molten Na_2CO_3-K_2CO_3-$CaCO_3$

View Article Online
DOI: 10.1039/D0GC02626C

The electrochemistry of molten carbonates was studied by cyclic voltammetry (CV) using a three-electrode setup contained in an alumina crucible that was filled with molten carbonates. The alumina crucible (inner diameter: 80 mm, height: 100 mm) was housed in a one-end-closed stainless steel (SS) test vessel protected by argon flow (99.99%, Shenyang Shuntai Special Gas Co., Ltd.). First, 450 g of the mixture of Na_2CO_3 and K_2CO_3 (Na: K = 59: 41, mol%) was dried under vacuum in the test vessel at 250 ^oC for 12 h. Then, the test vessel was filled with Ar and then was continuously flowed with Ar in the following steps. After that, the temperature was raised to 750 ^oC at 5 ^oC min^{-1} to melt the salt. Second, 50 g of $CaCO_3$ (99.9%, Sinopharm Chemical Reagent Co., Ltd) was added into the molten Na_2CO_3-K_2CO_3. After two hours, pre-electrolysis was performed between a nickel sheet cathode (1×2 cm) and a home-made Ni10Cu11Fe anode (diameter: 2 cm) under a constant cell voltage of 1.8 V for 2 h. Third, a copper wire (diameter: 1 mm), a silver wire (diameter: 1 mm) and the same Ni10Cu11Fe rod served as the working electrode, the pseudo-reference electrode, and the counter electrode, respectively. The CV measurement was performed at an electrochemical workstation (CH Instruments Inc., Shanghai, China, CHI1130a). All anhydrous $CaCO_3$, Na_2CO_3, K_2CO_3, $CaCl_2$, and CaO were analytical grade and purchased from Sinopharm Chemical Reagent Co., Ltd. A Ni10Cu11Fe anode (Ni: Cu: Fe = 79: 10 :11, weight ratio) was made by casting from liquid alloys prepared from the mixture of metal powders.

Electrolysis was conducted in a two-electrode system contained in the same setup as that was used for CV measurements. The Ni10Cu11Fe alloy rod and a nickel sheet served as the anode and the cathode, respectively, which were immersed in a molten $CaCO_3$-Na_2CO_3-K_2CO_3 electrolyte (Ca: Na: K = 23: 32: 45 mol%, eutectic at 665 ^oC). During electrolysis, the two-

View Article Online
DOI: 10.1039/D0GC02626C

electrode system was exposed in the CO_2 atmosphere. The power of the electrolysis processes was supplied by a battery testing system (Shenzhen Neware Co., Ltd, Shenzhen, China), and the operating temperatures of molten salt ranged from 710 to 850 ^oC. During the electrolysis, the outlet gases produced during electrolysis was monitored by gas chromatograph (FULI, 9790H). After electrolysis, the cathodic product was taken out from the molten salt, cooled down in the CO_2 atmosphere, and then transferred to the molten salt dissolver.

2.2 CaO dissolution in molten $CaCl_2$ and CO_2 absorption

The electrolytic products were soaked in molten $CaCl_2$ contained in an alumina crucible that was housed in a SS test vessel filled with argon, and the operating temperature was kept at 800 ^oC. Then, the soaked product was lifted from the molten salt, cooled down in the Ar atmosphere, washed with water, and vacuum-dried at 80 ^oC for 10 h. After soaking, CO_2 was directly bubbled into the molten $CaCl_2$ that had been used for soaking the electrolytic products. The flow rate of CO_2 was 40 mL min^{-1}. After absorption, the melt was cooled and dissolved in water to remove $CaCl_2$, and the residue was dried for further characterization.

To qualitatively measure the CO_2 absorption capability of molten $CaCl_2$-CaO, an absorption cell was constructed in an Al_2O_3 crucible filled with 100 g of $CaCl_2$ containing 1 wt% and 3 wt% CaO, respectively. The absorption process was conducted in a closed SS reactor at 800 ^oC and CO_2 gas was injected through the top of the sealed reactor with a flow rate of 40 mL min^{-1}. The electrolyte was sampled to analyze the $CaCO_3$ concentration after 10 min, 30 min, 1 h, 3 h, and 5 h, respectively. The absorptive amount of carbon dioxide is calculated based on the amount of calcium carbonate in the molten salt (Equation 1).

View Article Online
DOI: 10.1039/D0GC02626C

Carbonization reaction: $CaO_{(l)} + CO_{2(g)} = CaCO_{3(l)}$ (1)

2.3 Characterization

The crystal structures of all products were characterized by X-ray diffraction (XRD, Shimadzu X-ray 6000 with Cu Kα1 radiation at λ=1.5405 Å) and confocal Raman microspectroscopy (HR800, 100-240V 50/60Hz 488nm 100mw). Their morphologies were characterized by scanning electron microscopy (SEM, FEI Quanta FEG 250) equipped with EDS detector. Besides, the specific surface area of the electrolytic carbon was measured by Brunauer-Emmett-Teller analysis (BET, Quantachrome NOVA 1200e, Surface Area & Pore Size Analyzer). The procedure of assembling half-type coin cells and measuring the sodium-storage performance of electrolytic carbons was described in Supporting Information.

3. Results and discussions

3.1 Electrochemistry of $CaCO_3$

$CaCO_3$ is rich in the earth's crust, not only serving as a low-cost feedstock for making commodity chemicals but also a huge CO_2 reservoir. High-temperature molten carbonates can dissolve $CaCO_3$ and provide a wide electrochemical window to allow the electrochemical reduction of $CaCO_3$ (**Fig. 1a**). After electrolysis, the solid product of the mixture of C and CaO can be separated by dissolving CaO into molten $CaCl_2$ because of the high solubility of CaO in the molten $CaCl_2$[27, 28] (**Figs. 1b-c**). Then, the as-received $CaCl_2$-CaO melt is able to absorb CO_2 through the carbonization reaction without the passivation effect caused by the formation of the CaO@$CaCO_3$ core-shell structure because both CaO and $CaCO_3$ are highly soluble in the

View Article Online
DOI: 10.1039/D0GC02626C

molten $CaCl_2$ (**Fig. 1d**)[27, 28]. At last, $CaCl_2$ and $CaCO_3$ are recycled by a water-leaching process, whereby the $CaCO_3$ is insoluble in water while the $CaCl_2$ is highly soluble (**Fig. 1e**). Therefore, $CaCO_3$ act as a mediator to enable the electrolysis of CO_2 to produce C and O_2.

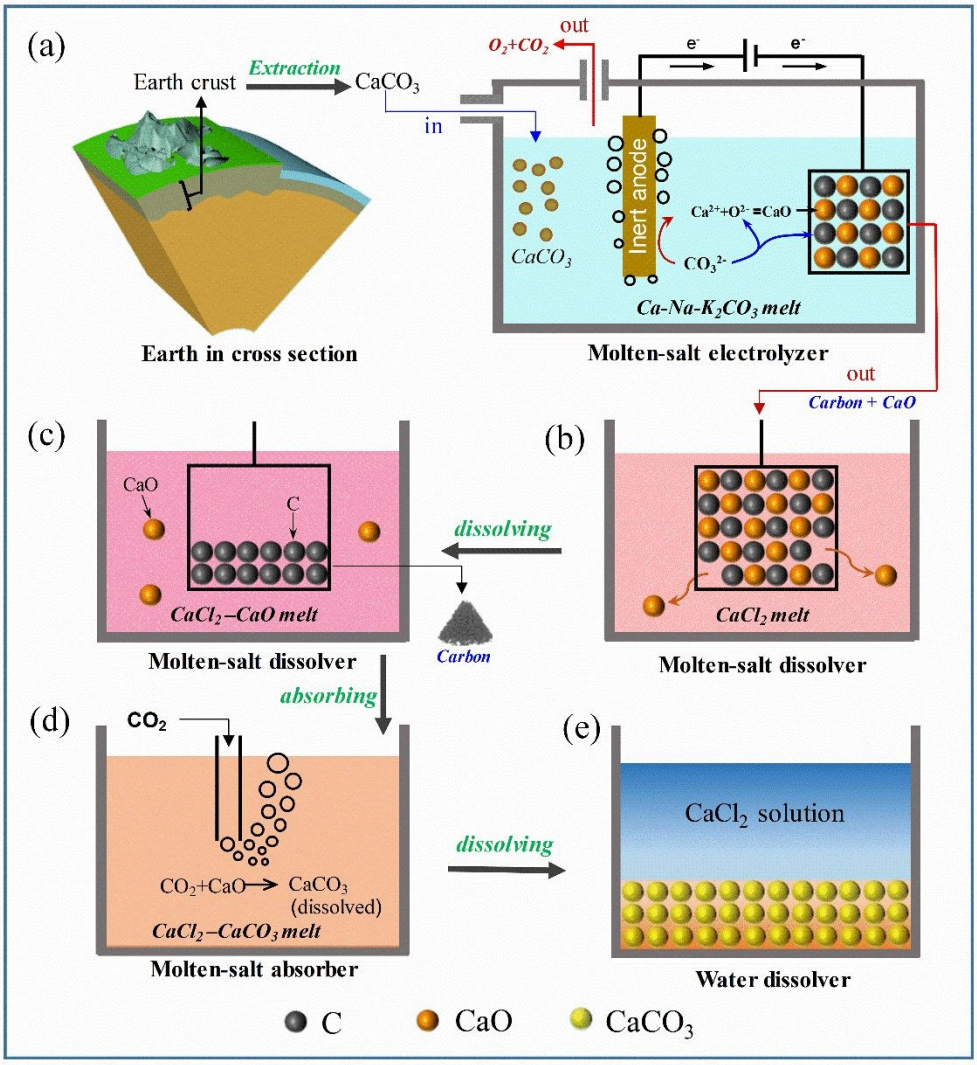

Fig. 1. Schematic illustration of the molten calcium carbonate mediator for the electrochemical reduction and absorption of carbon dioxide.

$CaCO_3$ rather than Li_2CO_3 is chosen as the active carbonate species due to thermodynamic considerations, resource abundance, and cost. As shown in **Fig. 2a**, lithium has the lowest abundance while the highest price among Na-, K-, and Ca-carbonates, i. e, the price of Li_2CO_3 is 100 times higher than that of $CaCO_3$ while the abundance of lithium is only 1/2500 of calcium.

View Article Online
DOI: 10.1039/D0GC02626C

Thus, the electrochemical reduction of $CaCO_3$ in the lithium-free carbonate is more practically viable than in the commonly used Li-containing molten salts (**Tab. S1**). In molten Na_2CO_3-K_2CO_3-$CaCO_3$, $CaCO_3$ is the electro-active species that can be reduced because it has been proven that carbonate ions cannot be reduced to carbon in Na_2CO_3-K_2CO_3[20, 29, 30]. In this regard, the electrolysis only consumes $CaCO_3$ (**Fig. 2b**) while Na_2CO_3-K_2CO_3 acts as the supporting electrolyte. Like Li_2CO_3, $CaCO_3$ can be reduced to carbon at a potential of 1.5V more positive than the deposition of Ca (**Fig. 2c**), thermodynamically convincing $CaCO_3$ as the electro-active species. After adding $CaCO_3$ into molten Na_2CO_3-K_2CO_3, a reduction peak (-1.4 V *vs.* Ag) prior to the Na deposition (-1.8 V *vs.* Ag) is due to the reduction of $CaCO_3$ (**Fig. 2d**). Thus, $CaCO_3$ can be reduced in the lithium-free molten carbonates.

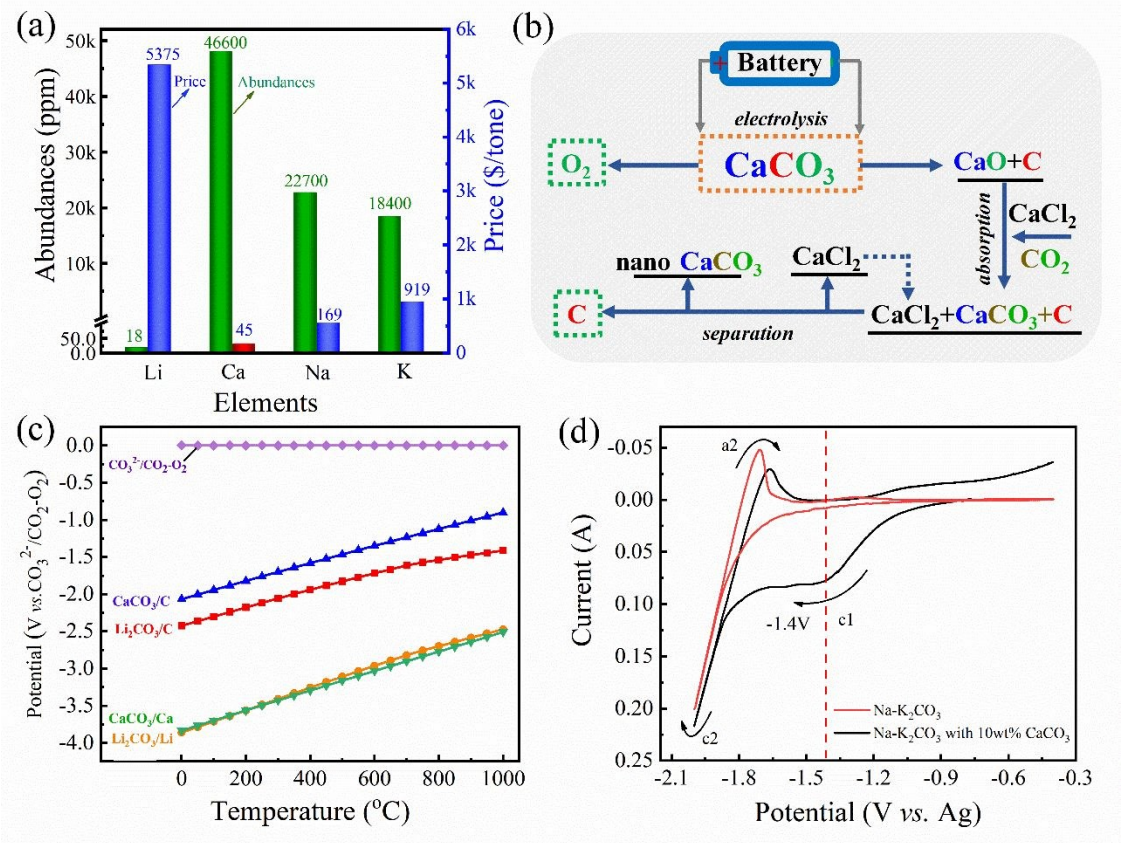

Fig. 2. (a) Profiles of the abundances of Li, Na, K, and Ca in the Earth's crust and the price of their corresponding carbonates, data derived from the reference[31]. (b) Flowsheet of a molten

View Article Online
DOI: 10.1039/D0GC02626C

$CaCO_3$ mediator for the electrochemical reduction and absorption of carbon dioxide. (c) Standard potential profiles of Li_2CO_3 and $CaCO_3$ as a function of temperature, all thermodynamic data are obtained from HSC Chemistry 6.0 and the activity of all involved species is at unit 1. (d) Cyclic voltammograms recorded from a Cu electrode in Na_2CO_3-K_2CO_3-10 wt% $CaCO_3$ melts at 750 °C under Ar atmosphere.

3.2 Electrolysis of molten $CaCO_3$-Na_2CO_3-K_2CO_3

The electrolysis of molten $CaCO_3$-Na_2CO_3-K_2CO_3 is to electrochemically splits $CaCO_3$ to carbon and CaO at the cathode and to oxygen at the Ni10Cu11Fe inert anode. According to the phase diagram of $CaCO_3$-Na_2CO_3-K_2CO_3[32], ~20wt% of $CaCO_3$ can be dissolved in the Na_2CO_3-K_2CO_3 eutectic at ~665 °C, which ensures a rapid mass transfer rate during the electrolysis. The electrolytic carbons obtained in molten $CaCO_3$-Na_2CO_3-K_2CO_3 are amorphous at 710 and 750 °C, and the amorphous carbon starts to graphitize when increasing the temperature to 800 and 850 °C (**Fig. 3a**). However, the amorphous carbon cannot be fully converted to graphite at 850 °C, which is different from the electrochemical conversion of amorphous carbon to graphite in molten $CaCl_2$ that reported by Jin et al[33]. It has also been observed that the amorphous carbon cannot be converted to graphite in molten NaCl-KCl-$MgCl_2$ at 650 °C[34, 35]. Thus, the composition of molten salt, operating temperature, and electrolysis parameters determine the graphitization of amorphous carbon. In addition, Raman spectra of electrolytic carbons also suggest that a higher operating temperature leads to the higher degree of graphitization that is reflected by the I_D:I_G ratios (I_D: I_G refers the intensity ratio of the D band and the G band) (**Fig. 3b**). In addition to operating temperatures, the degree of graphitization is also determined by

View Article Online
DOI: 10.1039/D0GC02626C

the cell voltage, i.e., electrolytic carbons obtained at a lower cell voltage has a higher degree of graphitization **(Figs. S1a-b)**. The degree of graphitization could relate to the growth rate of carbon and the interplay between the carbon and metals produced from side reactions caused by relatively high cell voltages. In addition, electrolytic carbons have a variety of morphologies, containing carbon sheets, particles, spheres, etc (**Figs. 3c-f)**.

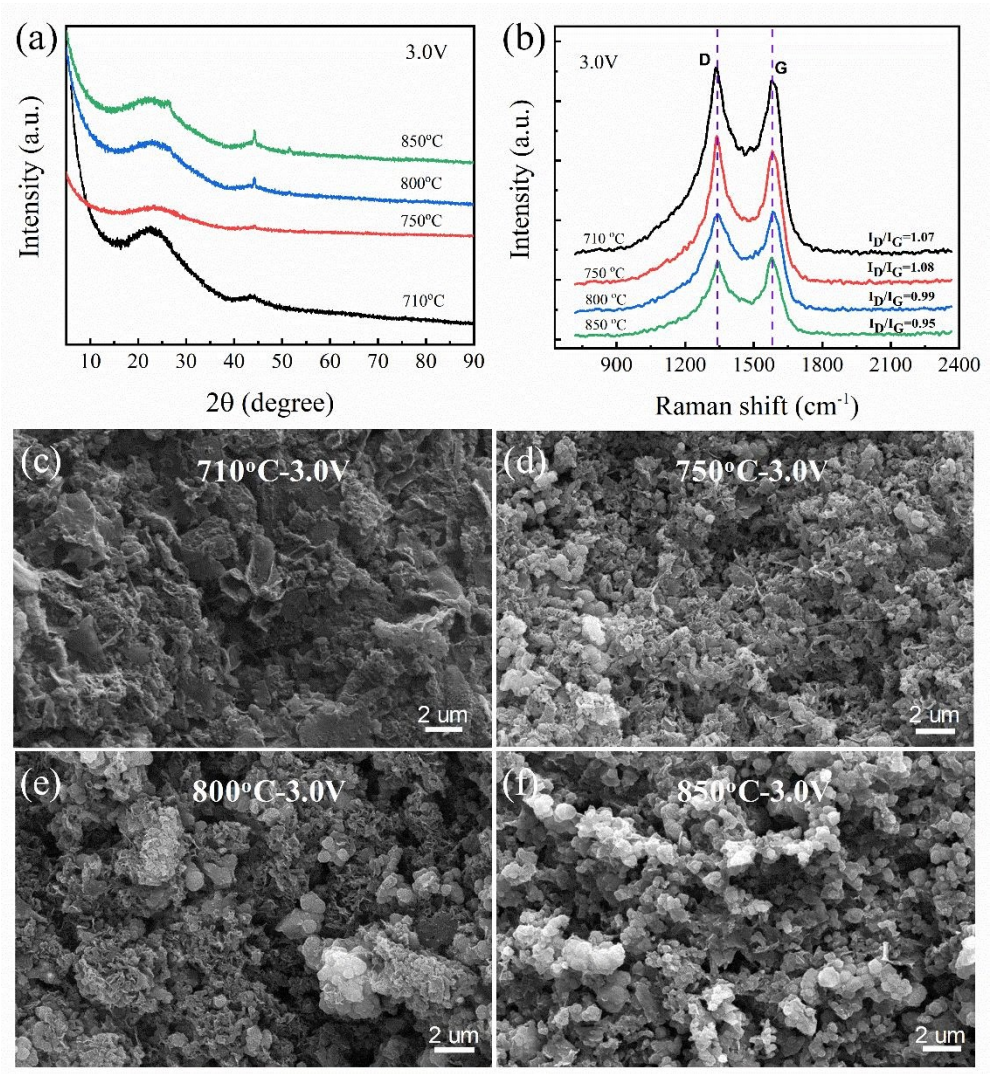

Fig. 3. (a-b) XRD patterns (a) and (b) Raman spectra of the electrolytic carbons obtained at 3.0 V in molten $CaCO_3$-Na_2CO_3-K_2CO_3 at operating temperatures ranging from 710 to 850 °C. (c-f) SEM images of the electrolytic carbons obtained at 3.0 V at (c) 710, (d) 750, (e) 800 and (f) 850 °C, respectively.

View Article Online
DOI: 10.1039/D0GC02626C

A cost–affordable and durable oxygen-evolution inert anode is crucial to enable the reduction of CO_2 rather than electro-refining carbon if a carbon electrode was used. The Ni10Cu11Fe alloy has been proven to be a low-cost and long-lasting inert anode in molten Na_2CO_3-K_2CO_3[14, 38, 39]. Recently, Wang et al. revealed that the stability of the Ni-based inert anodes was determined by the operating temperatures in molten Li_2CO_3-Na_2CO_3-K_2CO_3[40]. The Ni-based anode is a stable oxygen-evolution anode in molten Li_2CO_3-Na_2CO_3-K_2CO_3 when the operating temperature is higher than 650 °C. Surprisingly, the Ni10Cu11Fe is a stable oxygen-evolution inert anode in molten $CaCO_3$-Na_2CO_3-K_2CO_3. After working as an anode in molten $CaCO_3$-Na_2CO_3-K_2CO_3 for 100 h, the dimension of the anode does not change while a black oxide scale forms at the surface of the anode (the inset of **Fig. 4a**). The black oxide scale consists of NiO and $NiFe_2O_4$ (**Fig. 4b**), which agrees well with that obtained in molten Na_2CO_3-K_2CO_3[38]. The stability of the anode is due to the good electrical conductivity and chemical stability of spinal $NiFe_2O_4$ that has been proven to be an excellent inert anode material in the molten salts[41, 42]. Thus, the inertness of the anode is due to the formation of an oxide scale which enables oxygen evolution (**Fig. 4a**). From the cross-section SEM of the alloy (**Fig. 4c**), a dense oxide scale with a thickness of ~100 μm formed on the surface of the alloy substrate. From the results of linear scan analysis (inset of **Figs. 4c**, **e**), the concentration in the outermost layer has the highest oxygen and iron concentration, indicating that the Fe- and oxide-rich region mainly consists of $NiFe_2O_4$. Moreover, a thin copper-rich region was observed between the oxide scale and the alloy substrate, which is beneficial to strengthen the connection of the oxide scale and bulk metal[39]. According to the EDS analysis, the structure of the oxide scale is shown in **Fig.**

View Article Online
DOI: 10.1039/D0GC02626C

4d. Thus, the electrochemical reactions take place at the cathode and the anode can be expressed as equations 2-3.

Cathode reaction: $CaCO_3 + 4e^- = C + CaO + 2O^{2-}$ (2)

Anode reaction: $2CaCO_3 - 4e^- = 2Ca^{2+} + 2CO_2(g) + O_2(g)$ (3)

The overall reaction can be expressed as equation 4.

Overall reaction: $3CaCO_3 = 3CaO + C + 2CO_2(g) + O_2(g)$ (4)

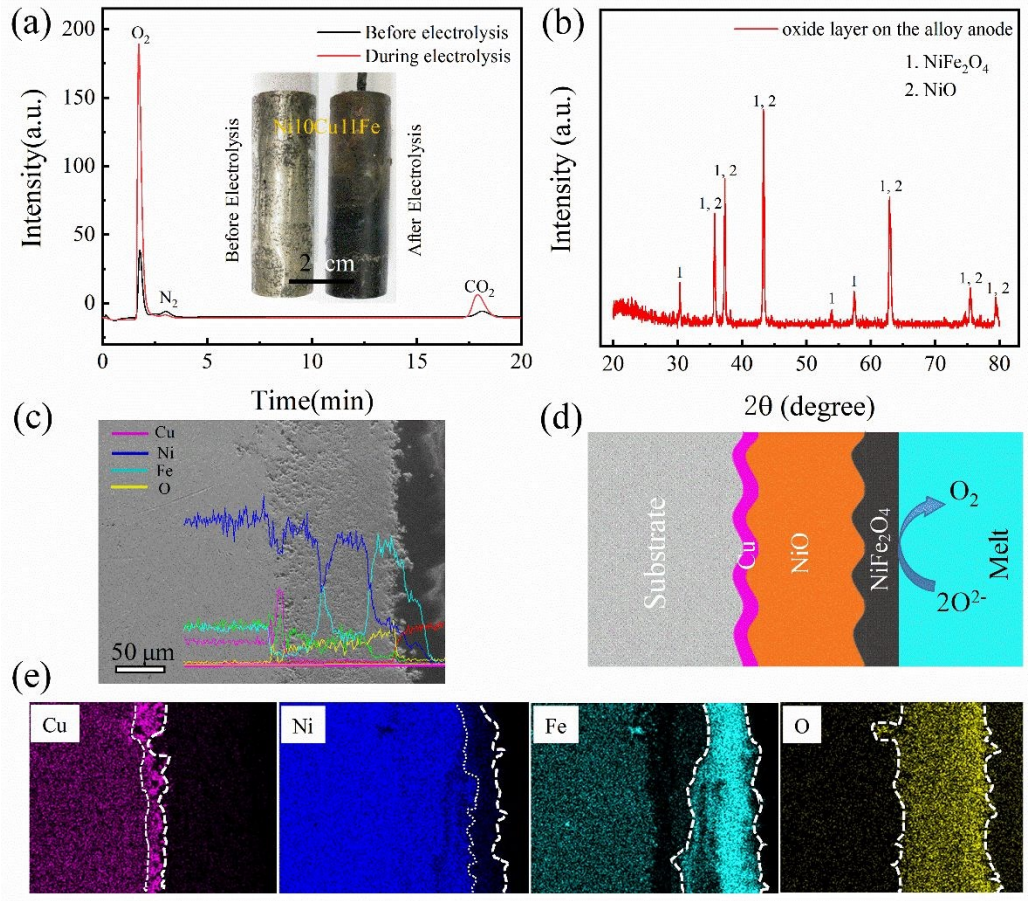

Fig. 4. (a) Gas chromatograms of the outlet gas before and during electrolysis using the Ni10Cu11Fe anode, the inset pictures are digital photos of Ni10Cu11Fe electrode before and after electrolysis. (b) XRD pattern of the oxide scale from the Ni10Cu11Fe alloy. (c) Cross-sectional SEM images and their corresponding linear concentration profiles of each element

View Article Online
DOI: 10.1039/D0GC02626C

across the interface of the alloy/oxide scale interface. (d) Schematic of the structure of the interface of alloy/oxide scale. (e) EDS mapping images of the interface of the alloy/oxide scale interface.

Current efficiency and energy consumption are measured by the collected carbon and consumed electricity. The current efficiency is an indicator of the selectivity of the electrochemical reactions. Among various conditions, the current efficiency ranges from 76.0% to 98.9% (**Fig. 5a**), and the highest current efficiency of the electrolysis is obtained under 800 ^{o}C at 2.8V for 3 h (inset of **Fig. 5a**). The current efficiency decreases when the cell voltage is higher than 3.0 V because a higher voltage may trigger side reactions such as co-deposition of sodium. The energy consumption increases with increasing the electrolysis voltage, and the minimum energy consumption for producing 1 kg of carbon ranges from 20.6 to 34.0 kW h of electrical energy (**Fig. 5b**). So, the cost of electricity for producing 1 kg of electrolytic carbon ranges 0.8 to 1.4 US$ assuming that the cost of electricity is US$0.04 kW h^{-13}. Note that the electricity for powering the furnace is not considered.

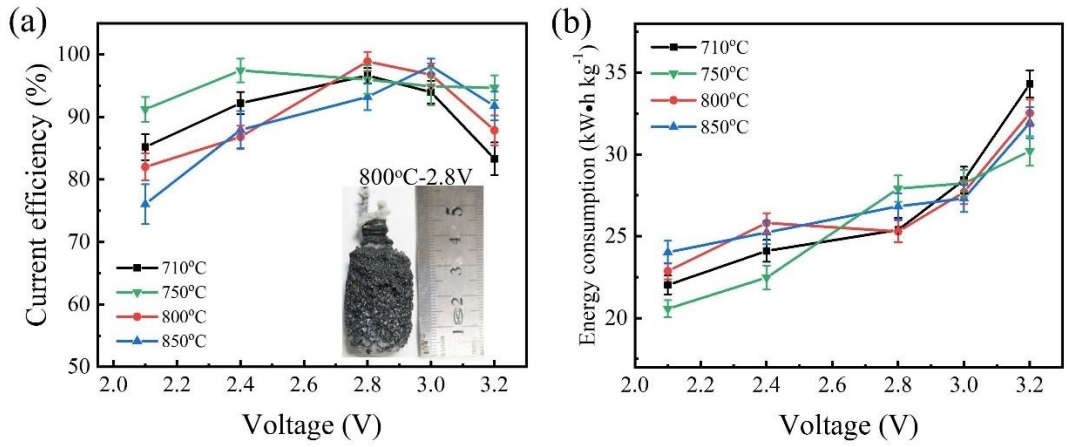

Fig. 5. (a) Profiles of current efficiency as a function of cell voltage in molten $CaCO_3$-Na_2CO_3-

View Article Online
DOI: 10.1039/D0GC02626C

K_2CO_3 at 710, 750, 800, and 850 °C, respectively. (b) Profiles of energy consumption as a function of the cell voltage at 710, 750, 800, and 850 °C, respectively.

3.3 Absorption of the CO_2 in molten $CaCl_2$-CaO melt

As shown in **Fig. S2**, the electrolytic products obtained from molten $CaCO_3$-Na_2CO_3-K_2CO_3 consists of CaO, $CaCO_3$ and a small quantity of $(Na, K)_2CO_3$ (the obvious characteristic peaks of electrolytic carbons was not observed in the XRD analysis due to an amorphous structure of electrolytic carbons) (**Fig. S2f**). Because CaO and $CaCO_3$ are insoluble in water, the electrolytic product wrapped in nickel foam was firstly soaked in molten $CaCl_2$ to dissolve CaO and $CaCO_3$ (**Fig. S2b**). Unlike the conventional way of separating CaO and $CaCO_3$ in mineral acid solutions, the CaO and $CaCO_3$ are soluble in molten $CaCl_2$, which are then separated from the electrolytic carbon. After the CaO and carbonate dissolved in molten $CaCl_2$ (**Fig. S2c, d**), the electrolytic carbons automatically peeled off from the nickel sheet (**Fig. S2e**). Since CaO is a well-known solid-absorbent for the capture of CO_2[43, 44], the dissolved CaO has a higher activity to combine with CO_2 through a rapid gas-liquid-conversion process in the molten salt without the deactivation effect caused by the $CaCO_3$ layer[45]. The soluble CaO in molten salts has a fast absorption capacity for CO_2 and **99%** of CaO can be converted to $CaCO_3$ within 30 min in the molten $CaCl_2$ containing 1 wt% or 3 wt% CaO **(Fig. 6a)**. After absorption, the quenched salt was dissolved in water and the insoluble product was $CaCO_3$ (**Fig. 6b**), further indicating that CaO had been completely converted to $CaCO_3$. Thus, molten $CaCl_2$ is a good solvent to dissolve CaO, and the obtained $CaCl_2$-CaO is capable of absorbing CO_2, regenerating $CaCO_3$ and thereby making $CaCO_3$ as a mediator. Therefore, the net reaction is

View Article Online
DOI: 10.1039/D0GC02626C

electrochemically splitting CO_2 to C and O_2.

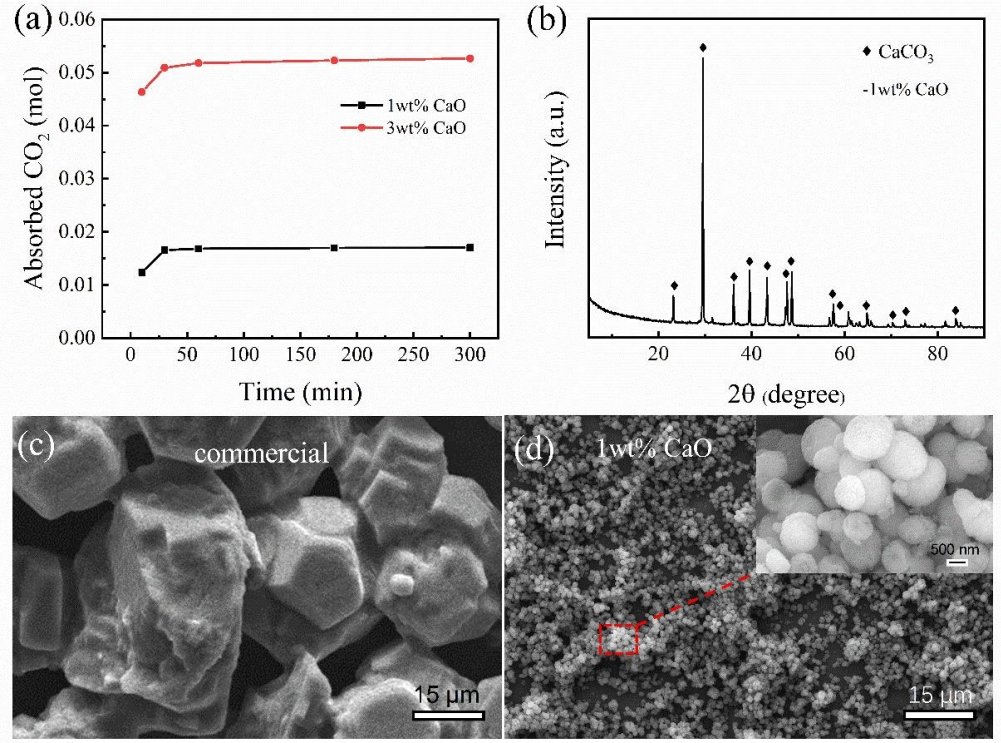

Fig. 6. (a) Profiles of CO_2 absorption as a function of time in molten $CaCl_2$ with 1 wt% and 3 wt% CaO, respectively. (b) XRD pattern of the insoluble solid product obtained by dissolving $CaCl_2$-1 wt% CaO in water. (c-d) SEM images of (c) commercial $CaCO_3$ and (d) $CaCO_3$ derived by dissolving $CaCl_2$-$CaCO_3$ in water.

The separation of $CaCO_3$ from the solidified $CaCl_2$-$CaCO_3$ is accomplished by a water-leaching process, which provides us a delicate approach to downsizing particles through a chemical etching process in water. At high temperatures, molten $CaCl_2$-$CaCO_3$ is a single phase because $CaCO_3$ is highly soluble in molten $CaCl_2$, while $CaCl_2$ and $CaCO_3$ exist in two different phases in water. The particle size of $CaCO_3$ feedstock is bigger than 20 μm (**Fig. 6c**), and the particle size of the obtained $CaCO_3$ is reduced to 500~800 nm (**Fig. 6d**). Moreover, the particle size and morphology of $CaCO_3$ vary with increasing the concentration of $CaCO_3$ in the molten $CaCl_2$. The sphere-like $CaCO_3$ was obtained from dissolving $CaCl_2$-1 wt% CaO and the rod-

View Article Online
DOI: 10.1039/D0GC02626C

and sheet-like $CaCO_3$ was obtained from dissolving $CaCl_2$-3 wt% and 5 wt% CaO in water, respectively. Note that the dimensions of both $CaCO_3$ rods and sheets were less than 5 μm (**Fig. S3**), meaning that the template-removing process significantly reduces the particle size and tailors the morphologies of $CaCO_3$ by tuning the $CaCO_3$ concentration in molten $CaCl_2$. As we know, the ultrafine calcium carbonate has been widely used as additives, medicine, food, etc[46, 47]. Compared with the currently deployed methods involving multiple steps, complex synthesis parameters[47, 48], the molten salt approach could open a radically different door to synthesizing micro- and nano-$CaCO_3$ in an efficient and green manner.

Fig. 7 illustrates the concept of tuning the particle size and morphology of $CaCO_3$ through a concept of salt-soluble-water-insoluble approach. First, $CaCO_3$ dissolves in molten $CaCl_2$, forming a homogeneous liquid phase (**Fig. 7a**). In the subsequent quenching process, $CaCl_2$ and $CaCO_3$ begin to co-crystallize to form a solid phase where $CaCO_3$ and $CaCl_2$ are mixed at an atomic scale (**Fig. 7a**). In this scenario, $CaCO_3$ distributes in the $CaCl_2$ matrix (**Fig. 7b**). In other words, $CaCl_2$ serves as the template that can be removed to tailor the structure and morphologies of $CaCO_3$. The elegance of this approach takes advantage of using different solubilities of $CaCO_3$ in molten $CaCl_2$ and water, and the $CaCl_2$ template can be etched by the low-cost and environmentally friendly water. In addition to $CaCO_3$, this approach can be used to prepare various functional materials based on the different solubilities in different media.

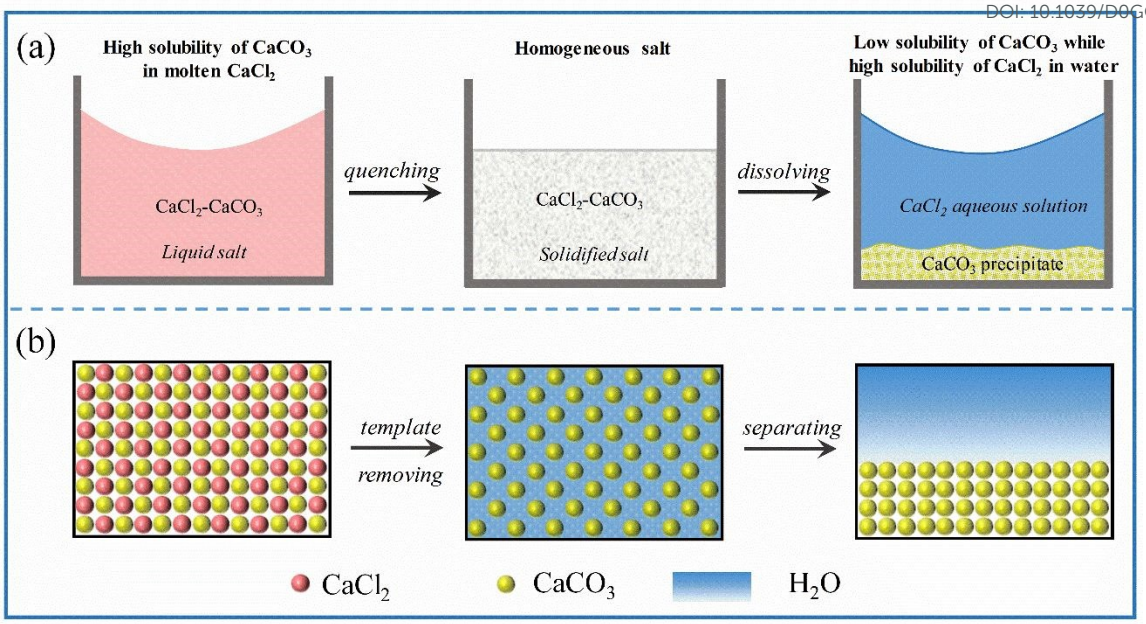

Fig. 7. (a) Schematic of the process to tailor the particle size of $CaCO_3$ using salt-to-water conversion process, and (b) the proposed mechanistic illustration of the salt-to-water conversion process.

3.4 Sodium-storage performance of electrolytic carbons

Electrolytic carbons show good sodium-storage performances. The electrolytic carbon obtained at 710 °C and 3.0 V is denoted as EC-710-3.0. A reduction peak at ~0.41 V (*vs.* Na^+/Na) is due to the formation of an solid electrolyte interface (SEI) film[36], and the sharp cathodic peak at 0.005 V (*vs.* Na^+/Na) and the anodic peak at 0.2 V (*vs.* Na^+/Na) are attributed to the reversible insertion/extraction of Na^+ from the graphited phase (**Fig. S4a**)[37]. The feature of a rectangular-shape CVs indicates a capacitive behavior of the carbon electrode, and the capacitive contributions account for 84% of the capacity (**Fig. S5**). The first discharge capacity of the EC-710-3.0 is 236.0 mAh g^{-1} with a Coulombic efficiency of 34.3% in sodium-ion batteries (denoted as SIBs) (**Fig. S4b**). The low Coulombic efficiency could be resulted from the large

View Article Online
DOI: 10.1039/D0GC02626C

surface area (**Fig. S6**), which could be improved by a post-heat treatment. Moreover, the EC-710-3.0 delivers 142.8 mAh g^{-1} at 1000 mA g^{-1} (**Fig. S4c**), and exhibits excellent cycling stability, i.e., the discharge capacity remains 210 mAh g^{-1} at 100 mA g^{-1} after 500 cycles with a capacity retention rate of 89.0% (**Fig. S4d**). The sodium-storage capacity of electrolytic carbons decreases with increasing the temperature of electrolysis (**Fig. S7a, Tab. S4**), which could relate to the particle size and specific surface area of electrolytic carbons (**Fig. S6**).

4. Conclusions

A molten Na_2CO_3-K_2CO_3-$CaCO_3$ carbonate electrolyzer can transform $CaCO_3$ into carbon and CaO at the cathode and O_2 at the Ni10Cu11Fe inert anode with a current efficiency of over 90%. Instead of electrochemically reducing CO_2, $CaCO_3$ is a CO_2 carrier being reduced in the form of CO_3^{2-} that has a high solubility in molten Na_2CO_3-K_2CO_3-$CaCO_3$. The electrolytic CaO and carbon can be separated by a molten $CaCl_2$-soaking process, by which CaO dissolves in molten $CaCl_2$ forming $CaCl_2$-CaO melts. The $CaCl_2$-CaO can be either used to capture CO_2 to form $CaCl_2$-$CaCO_3$ melts, or to be directly used for producing $Ca(OH)_2$ that is a key material for cement production. In addition, a concept of salt-soluble-water-insoluble approach has been proven as an effective approach to tailoring the particle size and morphologies of $CaCO_3$, thereby opening a new pathway to synthesize $CaCO_3$ with tunable particle sizes and structures. Further, electrolytic carbons are potential sodium-storage anode candidates that deliver a specific capacity of ~210 mAh g^{-1} at 100 mA g^{-1} after 500 cycles with a capacity retention of 89.0%. Considering the huge limestone deposit and the ever-decreasing price of renewable-powered electricity, the electrolysis of molten $CaCO_3$ offers new opportunities for the

View Article Online
DOI: 10.1039/D0GC02626C

valorization of CO_2, preparation of energy storage materials and oxygen, production of clean cement, and fabricating of functional $CaCO_3$.

Acknowledgments

We greatly thank the financial support from the Fundamental Research Funds for the Central Universities (N2025035), Xingliao Project (XLYC1807042), and the 111 Project (B16009).

References

1. J. Kleypas, R. Buddemeier, D. Archer, J. Gattuso, C. Langdon, B. Opdyke, *Science*, 1999, **284**, 118-120.

2. S. Chu and A. Majumdar, *Nature*, 2012, **488**, 294-303.

3. S. Chu, Y. Cui, N. Liu, *Nat. Mater.* 2017, **16**, 16-22.

4. C. Chen, J. F. K. Kotyk, S. W. Sheehan, *Chem.* 2018, **4**, 2571-2586.

5. S. Nitopi, E. Bertheussen, S. B. Scott, X. Liu, A. K. Engstfeld, S. Horch, B. Seger, I. E. Stephens, K. Chan, C. Hahn, *Chem. Rev.* 2019, **119**, 7610-7672.

6. Z. Sun, T. Ma, H. Tao, Q. Fan, B. Han, *Chem.* 2017, **3**, 560-587.

7. M. Ross, P. De Luna, Y. Li, C. Dinh, D. Kim, P. Yang, E. Sargent, *Nat. Catal.* 2019, **2**, 648-658.

8. C.-T. Dinh, T. Burdyny, M. G. Kibria, A. Seifitokaldani, C. M. Gabardo, F. P. G. De Arquer, A. Kiani, J. P. Edwards, P. De Luna and O. S. Bushuyev, *Science,* 2018, **360**, 783-787.

View Article Online
DOI: 10.1039/D0GC02626C

9. A. Bakac, John Wiley & Sons, 2010.

10. P. Macreadie, O. Serrano, D. Maher, C. Duarte, J. Beardall, *Limnology and Oceanography Letters,* 2017, **2** (6), 195-201.

11. L. Ellis, A. Badel, M. Chiang, R. Park, Y. J. *Proc. Natl. Acad. Sci.* Chiang, 2019, **117**, 12584-12591.

12. H. Groult, B. Kaplan, S. Komaba, N. Kumagai, V. Gupta, T. Nakajima and B. *J. Electrochem. Soc.* 2003, **150**, G67-G75.

13. S. Licht, B. Wang, S. Ghosh, H. Ayub, D. Jiang, J. Ganley, *J. Phys. Chem. Lett.* 2010, **1**, 2363-2368.

14. H. Yin, X. Mao, D. Tang, W. Xiao, L. Xing, H. Zhu, D. Wang, D. R. Sadoway. *Energy Environ. Sci.* 2013, **6**, 1538-1545.

15. K. Otake, H. Kinoshita, T. Kikuchi, R. Suzuki, *Electrochim. Acta.* 2013, **100**, 293-299.

16. W. Weng, L. Tang, W. Xiao, *J. Energy Chem.* 2019, **28**, 128-143.

17. F. Li, S. Liu, B. Cui, J. Lau, J. Stuart, B. Wang, S. Licht, *Adv. Energy Mater.* 2015, **5**, 1401791, 1-7.

18. H. Wu, D. Ji, L. Li, D. Yuan, Y. Zhu, B. Wang, Z. Zhang, S. Licht, *Adv. Mater. Technol.* 2016, **1**, 1600092.

19. P. Claes, D. Moyaux, D. J. Peeters, *Eur. J. Inorg.Chem.* 1999, **(4)**, 583-588.

20. M. Ingram, B. Baron, G. Janz, *Electrochim. Acta.* 1966, **11**, 1629-1639.

21. B. J. S. Swain. *Sep. Purif. Technol.* 2017, **172**, 388-403.

22. P. Choubey, M. Kim, R. Srivastava, J. Lee, J. Lee, *Miner. Eng.* 2016, **89**, 119-137.

23. Wilson J L. The lower carboniferous Waulsortian facies//Carbonate Facies in Geologic

View Article Online
DOI: 10.1039/D0GC02626C

History. Springer, New York, NY. **1975**, 148-168.

24. K. Zhang, Q. Li, L. Yan, L. Zeng, L. Lu, Y. Zhang, J. Hui, X. Jin, X. Tang, *Earth-Sci. Rev.* 2017, **167**, 27-46.

25. J. M. Matter, P. B. Kelemen, *Nat. Geosci.* 2009, **2**, 837-841.

26. S. Licht, H. Wu, C. Hettige, B. Wang, J. Asercion, J. Lau, J. Stuart, *Chem. Commun.* 2012, **48**, 6019-6021.

27. E. Freidina, D.Fray, *Thermochimica. Acta*. 2000, **351** (1-2), 107-108.

28. S. Wang, F. Zhang, X. Liu and L. Zhang, *Thermochim. Acta.* 2008, **470**, 105-107.

29. H. Yin, D. Tang, H. Zhu, Y. Zhang and D. Wang, *Electrochem. Commun.* 2011, **13**, 1521-1524.

30 A. Shatskiy, K. Litasov, Y. Palyanov, *Russian Geology and Geophysics*, 2015, **56**, 113-142.

31 Carmichael, R. S. Practical Handbook of Physcial Properties of Rocks and Minerals. CRC Press: Boca Raton, FL, 1989.

32. A. Cooper, J. Gittins and O. Tuttle, *Am. J. Sci.* 1975, **275**, 534-560.

33. J. Peng, N. Chen, R. He, Z. Wang, S. Dai, X. Jin, *Angew. Chem., Int. Ed.* 2017, **56**, 1751-1755.

34. Z. Zhao, H. Xie, J. Qu, H. Zhao, Q. Ma, P. Xing, Q. Song, D. Wang, H. Yin, *Batteries Supercaps*, 2019, **2**, 1007-1015.

35 X. Zhou, H. Xie, X. He, Z. Zhao, Q. Ma, M. Cai, H. Yin. *Energy Environment Materials*, 2019, **0**, 1-11.

36. Q. Jiang, Z. Zhang, S. Yin, Z. Guo, S. Wang, C. Feng, *Appl. Surf. Sci.* 2016, **379**, 73-82.

37. F. D. Han, Y. J. Bai, R. Liu, B. Yao, Y. X. Qi, N. Lun, X. Zhang, *Adv. Energy Mater.* 2011,

View Article Online
DOI: 10.1039/D0GC02626C

1, 798-801.

38. D. Tang, K. Zheng, H. Yin, X. Mao, D. R. Sadoway, D. Wang, *Electrochim. Acta.* 2018, **279**, 250-257.

39. X. Cheng, L. Fan, H. Yin, L. Liu, K. Du, D. Wang, *Corros. Sci.* 2016, **112**, 54-62.

40. K. Zheng, K. Du, X. Cheng, R. Jiang, B. Deng, H. Zhu, D. Wang, *J. Electrochem. Soc.* 2018, **165**, E572-E577.

41. L. Ma, K. Zhou, Z. Li, *Corros. Sci.* 2011, **53**, 2357-2367.

42 L. Ma, K. Zhou, Z. Li, Q. Wei, L. Zhang, *Corros. Sci.* 2011, **53**, 3712-3724.

43. M. Mohammadi, P. Lahijani, A. Mohamed, *Chem. Eng. J.* 2014, **243**, 455-464.

44. D. Karami, N. J. I. Mahinpey, *Ind. Eng. Chem. Res.* 2012, **51**, 4567-4572.

45. V. Tomkute, A. Solheim, E. Olsen, *Energy Fuels.* 2013, **27**, 5373-5379.

46. Y. Boyjoo, V. K. Pareek, J. Liu, *J. Mater. Chem. A.* 2014, **2**, 14270-14288.

47. H. Du, E. Amstad, *Angew. Chem., Int. Ed.* 2020, **59**, 1798-1816.

48 T. Zhao, B. Guo, F. Zhang, F. Sha, Q. Li, J. Zhang, *ACS Appl. Mater. Interfaces.* 2015, **7**, 15918-15927.

View Article Online
DOI: 10.1039/D0GC02626C

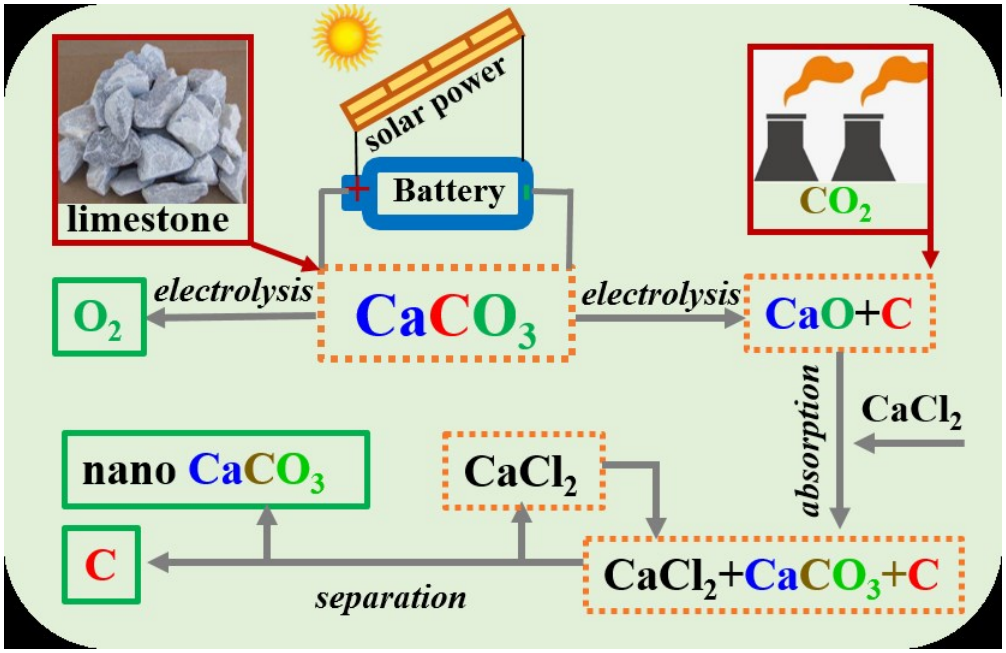

140x90mm (150 x 150 DPI)